The 21ˢᵗ International Congress on Sound and Vibration

13-17 July, 2014, Beijing/China

ICSV 21

13-17 July, 2014, Beijing/China

MODEL BASED CONTROL OF NONLINEAR COMBUSTION INSTABILITIES

Li Jingxuan, Morgans Aimee, S.

Department of Aeronautics, Imperial College London, London, UK, SW7 2AZ
e-mail: jingxuan.li@imperial.ac.uk

Lean premixed combustion chambers are susceptible to combustion instabilities arising from the coupling between the heat release rate perturbations and the acoustic disturbances. These instabilities are generally harmful. Active feedback control can be used to interrupt the coupling between the acoustic waves and unsteady heat release and prevent or suppress instability. The design of most types of controller requires prior knowledge of how the combustor responds to actuation - the "open loop transfer function" (OLTF). This includes the flame response to oncoming flow disturbances, which becomes non-linear at larger amplitudes. Saturation of the heat release rate amplitude or a phase lag change relative to the acoustic pressure as the modulation level increases has been confirmed to occur experimentally in many cases. This may cause the dominant unstable frequency to change, which in turn alters the OLTF and makes the design of controller more complicated. A flame describing function model is proposed in this paper to account for the non-linearities of the heat release rate amplitude. This flame model is applied to a model combustor. The ν-gap metric is used to quantify the deviation of the set of OLTFs for different disturbance levels from the selected transfer function for the controller design. This provides us a bound on the minimum required "robustness stability margin" for an $\mathcal{H}_\infty$ loop shaping controller. Such a controller is synthesized, and it is confirmed that as long as the ν-gap is smaller than the stability margin, the robust controller is guaranteed to stabilize the combustor for all possible flame responses.

1. Introduction

Combustion instabilities arise due to the coupling between the unstable combustion process and acoustic disturbances within the combustion chamber [1]. These instabilities are generally not desirable because they may lead to an early ageing of the combustion chamber or in extreme cases to severe structural damage [2].

The stability of a combustion chamber is determined by the balance between the energy gained from the heat released from unsteady combustion and various dissipation processes, such as acoustic losses [1], which are generally considered to be linear. However, nonlinear mechanisms dominate the dynamics of real unstable combustion systems. Saturation of the heat release rate amplitude or a phase lag change relative to the acoustic pressure (and hence a change in the Rayleigh source term $< p'\dot{q}' >$ driving combustion instabilities [3, 4]) with the modulation level have been experimentally identified in many cases [5, 6]. The presence of the nonlinear mechanisms thus makes feedback controller design more complicated. The "open loop transfer function" (OLTF)[4] between a monitored thermodynamic property within the combustion chamber and the actuator signal used for feedback

control changes during non-linear combustion instabilities. By basing controller design on a single OLTF (normally the one corresponding to small, linear disturbances), it then can not be guaranteed that the controller, will stabilize across all of the different disturbance levels. In particular, control activated from within the (non-linear) limit cycle is not guaranteed to be stabilising, although it is typically observed in practice that it is [18]. The ν-gap metric [7] is utilized in this work to quantify the deviation of the sets of OLTF from the selected plant for controller design, in the context of a feedback loop being present. This provides us a bound on the minimum required "robustness stability margin" for an $\mathcal{H}_\infty$ loop shaping controller [8].

The objective of this paper is to design a feedback controller which is guaranteed to stabilize a non-linear combustion system across all possible amplitude levels. This will be achieved by combining the $\mathcal{H}_\infty$ loop shaping synthesis with the ν-gap metric, so that as long as the ν-gap is smaller than the stability margin, the robust controller is guaranteed to stabilize the combustor for all possible flame responses.

The rest of the paper is organized as follows. The acoustic network and the non-linear combustion model are presented in Section 2. A governing matrix equation is derived to link the linear acoustic response of the Rijke tube with the non-linear response of the flame to velocity disturbances. The acoustic model is then converted into the time domain and connected with the proposed non-linear flame model in order to determine the time evolution of disturbances. A typical non-linear combustion instability case is selected and the design and application of the robust controller are shown in Section 3. Both frequency and time domain versions of simulation code are open source (OSCILOS), and are freely available (see `www3.imperial.ac.uk/people/a.morgans`). Conclusions are drawn in the final section.

2. Model of Rijke tube

2.1 Acoustic wave equations

Analysis is carried out on a simple model combustion chamber which is schematically described in Figure 1. The configuration consists of a cylindrical Rijke tube with both ends open. Denoting the distance along the tube axis by the vector x, the inlet and outlet of the tube are at $x = -x_1$ and $x = x_2$ respectively. A premixed gaseous flame located at $x = 0$ is used as the heat source. The fully mixed fresh gases are ignited and rapidly turn to burned gases. A loudspeaker is placed at the inlet of the tube as a control actuator and a microphone equipped downstream of the combustion zone with a distance $x = x_r$ is used as the sensor. In the analysis, the following assumptions are implemented: (1) The envisaged frequencies are assumed sufficiently small to consider the combustion zone to be "compact" compared to the acoustic wavelength and to only take into account the longitudinal waves. (2) The fluids before and after the combustion zone are assumed to be perfect gases. The specific heats c_p and c_v are considered constant. The temperature T can be expressed as the function of pressure p and density ρ. (3) The dissipation of acoustic waves throughout the tube is negligible and acoustic damping only happens at the ends of the tube. (4) There is no noise produced by the entropy waves formed during the unstable combustion process — these waves are assumed to leave the tube without interaction with the flow at the end of tube.

Now consider weak disturbances induced upstream of the combustion zone. Acoustic waves propagate in both directions and the flow is assumed to be isentropic upstream. The upstream and downstream regions are indicated by the subscripts 1 and 2. Taking the flow to be composed of a steady uniform mean flow (denoted as $^-$) and small perturbations (denoted as $'$), it is thus possible to
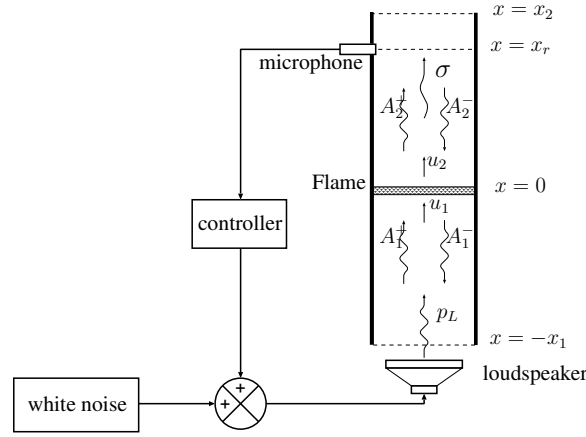
Figure 1. Schematic view of the Rijke tube and the control configuration.

write out the pressure and velocity in the upstream region [9]:

$$p_1(x,t) = \bar{p}_1 + A_1^+\left(t - \frac{x}{\bar{c}_1+\bar{u}_1}\right) + A_1^-\left(t + \frac{x}{\bar{c}_1-\bar{u}_1}\right) + p_L\left(t - \frac{x}{\bar{c}_1+\bar{u}_1}\right) \tag{1}$$

$$u_1(x,t) = \bar{u}_1 + \frac{1}{\bar{\rho}_1\bar{c}_1}\left[A_1^+\left(t - \frac{x}{\bar{c}_1+\bar{u}_1}\right) - A_1^-\left(t + \frac{x}{\bar{c}_1-\bar{u}_1}\right) + p_L\left(t - \frac{x}{\bar{c}_1+\bar{u}_1}\right)\right] \tag{2}$$

where $-x_1 \leq x < 0$. u and c represent the longitudinal velocity and speed of sound respectively. p_L indicates the sound signal from the loudspeaker. A_1^+ and A_1^- denotes the amplitude of the inward and outward propagating acoustic waves upstream of the flame respectively. Similarly, downstream of the combustion zone:

$$p_2(x,t) = \bar{p}_2 + A_2^+\left(t - \frac{x}{\bar{c}_2+\bar{u}_2}\right) + A_2^-\left(t + \frac{x}{\bar{c}_2-\bar{u}_2}\right) \tag{3}$$

$$u_2(x,t) = \bar{u}_2 + \frac{1}{\bar{\rho}_2\bar{c}_2}\left[A_2^+\left(t - \frac{x}{\bar{c}_2+\bar{u}_2}\right) - A_2^-\left(t + \frac{x}{\bar{c}_2-\bar{u}_2}\right)\right] \tag{4}$$

$$\rho_2(x,t) = \bar{\rho}_2 + \frac{1}{\bar{c}_2^2}\left[A_2^+\left(t - \frac{x}{\bar{c}_2+\bar{u}_2}\right) + A_2^-\left(t + \frac{x}{\bar{c}_2-\bar{u}_2}\right)\right] - \frac{\gamma\bar{p}_2}{\bar{c}_2^2}\sigma\left(t - \frac{x}{\bar{u}_2}\right) \tag{5}$$

where $0 < x \leq x_2$. A_2^+ and A_2^- represent the amplitudes of the outward and inward travelling waves after the flame respectively. σ denotes the amplitude of the entropy wave. The link between the inward and outward propagating waves can be described by the reflection coefficient at the boundary. The pressure reflection coefficients at the inlet and outlet are characterized by R_1 and R_2 respectively. The acoustic waves generated by the entropy wave can be neglected in this work as the interaction between the entropy wave and weak subsonic flow will be very small [10]. In order to relate the upstream and downstream acoustic waves, the mass, momentum and energy conservation equations across the flame zone are combined with the perfect gas equation to obtain two equations in the Laplace domain which are independent of ρ_2 (which contains the entropy component) [11]:

$$\begin{bmatrix} X_{11} & X_{12} \\ X_{21} & X_{22} \end{bmatrix}\begin{bmatrix} A_1^-(s) \\ A_2^+(s) \end{bmatrix} + \begin{bmatrix} Y_{11} & Y_{12} \\ Y_{21} & Y_{22} \end{bmatrix}\begin{bmatrix} R_1(s)A_1^-(s)e^{-\tau_1 s} + p_L(s)e^{-\tau_L s} \\ R_2(s)A_2^+(s)e^{-\tau_2 s} \end{bmatrix} = \begin{bmatrix} 0 \\ -1 \end{bmatrix}\frac{\dot{q}'(s)}{\bar{c}_1} \tag{6}$$

where $\tau_1 = 2x_1 \left/ \left(\bar{c}_1(1 - \bar{M}_1^2)\right)\right.$, $\tau_2 = 2x_2 \left/ \left(\bar{c}_2(1 - \bar{M}_2^2)\right)\right.$, $\tau_L = x_1 \left/ \left(\bar{c}_1(1 + \bar{M}_1)\right)\right.$, $M = u/c$ denotes the Mach number and $\dot{q}'$ indicates the heat release rate perturbations. To account for the radiation of sound at the end of the open tube, $R_i(s) = -\left(1 + 0.5(rs/\bar{c}_i)^2\right)e^{1.22(rs/\bar{c}_i)}$, $i = 1, 2$, where $r = 0.08$ m indicating the radius of the tube [12]. The expressions of the coefficients X_{ij} and Y_{ij} are

given as:

$$X_{11} = (1 - \bar{M}_1)(1 - \bar{M}_1 + \frac{\bar{c}_2}{\bar{c}_1}\bar{M}_2) \qquad\qquad X_{12} = -(1 + \bar{M}_2)$$

$$X_{21} = \frac{\gamma\bar{M}_1 - 1}{\gamma - 1} + \frac{1}{2}\bar{M}_1^2(\bar{M}_1 - 3) + \frac{1}{2}\frac{\bar{c}_2^2}{\bar{c}_1^2}\bar{M}_2^2(1 - \bar{M}_1) \qquad\qquad X_{22} = -\frac{\bar{c}_2}{\bar{c}_1}\left[\frac{\gamma\bar{M}_2 + 1}{\gamma - 1} + \bar{M}_2^2\right]$$

$$Y_{11} = (1 + \bar{M}_1)(1 + \bar{M}_1 - \frac{\bar{c}_2}{\bar{c}_1}\bar{M}_2) \qquad\qquad Y_{12} = -(1 - \bar{M}_2)$$

$$Y_{21} = \frac{\gamma\bar{M}_1 + 1}{\gamma - 1} + \frac{1}{2}\bar{M}_1^2(\bar{M}_1 + 3) - \frac{1}{2}\frac{\bar{c}_2^2}{\bar{c}_1^2}\bar{M}_2^2(1 + \bar{M}_1) \qquad\qquad Y_{32} = -\frac{\bar{c}_2}{\bar{c}_1}\left[\frac{\gamma\bar{M}_2 - 1}{\gamma - 1} - \bar{M}_2^2\right]$$

In order to obtain the amplitude coefficients $A_1^-(s)$ and $A_2^+(s)$, the flame model is induced to link the heat release rate with the upstream velocity perturbations.

2.2 Flame model

In this work, a simple model, which captures the flame response shape predicted by the G-equation for conical flames [13], is the famous $n - \tau$ model [14] filtered by a low pass filter:

$$\frac{\hat{\dot{q}}}{\bar{\dot{q}}}\Big/\frac{\hat{u}_1}{\bar{u}_1} = n_f e^{-\tau_f s} = a_f\left(\frac{\omega_c^2}{s^2 + 2\xi_c\omega_c s + \omega_c^2}\right)^2 e^{-\tau_f s} \tag{7}$$

where a_f is the gain of the filter, ω_c denotes the cut-off frequency and ξ_c represents the damping factor of the second order filter. The superscript ˆ indicates the amplitude of perturbed signal. The nonlinear model used in this work is similar to that in [15] but with important modifications. In [15], the saturation point of the heat release rate amplitude is the boundary point between the linear and non-linear regimes. However, this is not always the case and the nonlinearity may appear before saturation [16]. We therefore smooth the traditional describing function, using the mathematical description:

$$a_f = \int_0^{\hat{u}_1/\bar{u}_1} \frac{1}{1 + (\alpha + 0.85)^{30}} d\alpha \tag{8}$$

The exact form of the non-linear combustion model may not fully represent a real configuration, but does represent a simplified model which captures many realistic non-linear features and thus can be used to get a better understanding of combustion instabilities. Figure 2 shows the evolutions of the gain n_f and $\hat{\dot{q}}/\bar{\dot{q}}$ of the first mode with $\hat{u}_1/\bar{u}_1$. The parameters of the Rijke tube and flame model are specified in Table 1.

Table 1. Thermodynamic and flow conditions in the Rijke tube and parameters for the simulation.

$\bar{p}_1$ [Pa]	$\overline{T}_1$ [K]	$\overline{M}_1$ [-]	$\overline{T}_2/\overline{T}_1$ [-]	x_1 [m]	x_2 [m]	x_r [m]	ω_c [rad/s]	ξ_c
1×10^5	300	0.01	2	0.5	0.3	0.15	$2\pi \times 400$	0.707

3. Simulation of non-linear combustion instabilities and control

By substituting the flame model into equation 6, it is possible to calculate the eigenvalues $\theta_j + 2\pi f_j^* i$, $j = 1, 2, \ldots$ of the system, where f_j^* indicates the eigenfrequency of the jth mode and θ_j represents the corresponding growth rate. The growth rates can be used to identify the stability of the system. When $\theta_j > 0$, the jth mode is unstable. The eigenfrequencies and growth rates may change during non-linear combustion instabilities. Figure 3 shows the trajectory of the eigenfrequency and corresponding growth rate of the first mode of one test case. The time delay τ_f of the flame model equals 2 ms. Part of the trajectory of the first mode has a positive growth rate. The growth rate equals 32 rad/s when $\hat{u}_1/\bar{u}_1 = 0$, meaning that the first mode is unstable and weak disturbances increase
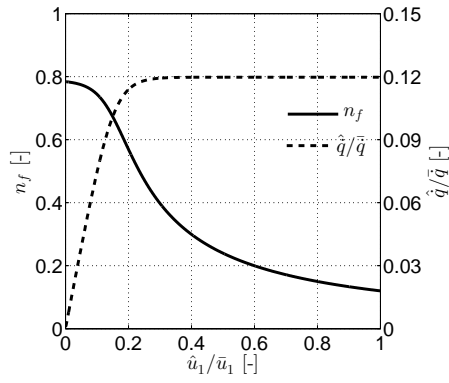
Figure 2. Plots of the $\hat{\dot{q}}/\bar{q}$ and n_f with $\hat{u}_1/\bar{u}_1$ for the first mode.
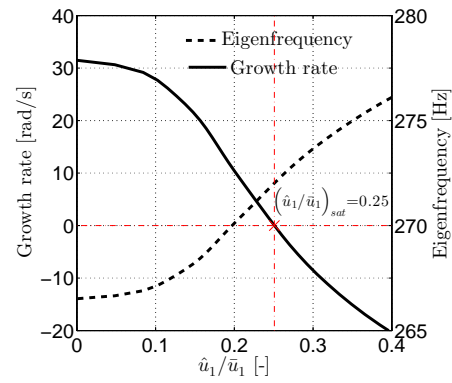
Figure 3. Evolutions of the eigenfrequency and corresponding growth rate of the first mode with $\hat{u}_1/\bar{u}_1$.

exponentially with an envelope of $\exp{(32t)}$. The growth rate decreases with $\hat{u}_1/\bar{u}_1$ and becomes zero when $\hat{u}_1/\bar{u}_1 = 0.25$, hence this is the velocity fluctuation amplitude at which we expect limit cycle oscillations to occur. Meanwhile, the eigenfrequency also changes with the growth of $\hat{u}_1/\bar{u}_1$.

The implied limit cycle is validated by the simulations in the time domain. The network is built using the Simulink environment and detailed configurations can be viewed in our recent contribution [17]. Non-linear combustion instabilities can be well reproduced and different controllers can be applied to this system. Figure 8 shows that the time evolution of the signals a_f, $\dot{q}'/\bar{q}$ and $u_1'/\bar{u}_1$. $\dot{q}'/\bar{q}$ and $u_1'/\bar{u}_1$ oscillate as sinusoidal waves. The evolution of oscillating frequency can be resolved from the time-frequency analysis of the signal $u_1'/\bar{u}_1$ shown at the bottom of Fig. 8. With the growth of $\hat{u}_1/\bar{u}_1$, the signals oscillate at frequency of approx 270 Hz and a limit cycle in $\dot{q}'/\bar{q}$ and $u_1'/\bar{u}_1$ is established for the first mode.

3.1 Open loop transfer function

The open loop transfer function (OLTF) for control purposes is from the sound signal p_L produced by the loudspeaker to the signal p_r measured by the reference microphone. The profile of the OLTF changes with the amplitude of the inlet velocity perturbations $\hat{u}_1/\bar{u}_1$ due to non-linearity. Note that the assumption of "weak nonlinearity" has been made: this assumes that the output harmonic content contains the same frequency as the input harmonic content, but with a gain and phase shift that is amplitude, as well as frequency dependent. In practical unstable combustion system, measurement of the OLTF is complicated since the non-linear limit cycle dominates during the combustion instability. To overcome this problem, a loudspeaker signal is used which contains two components
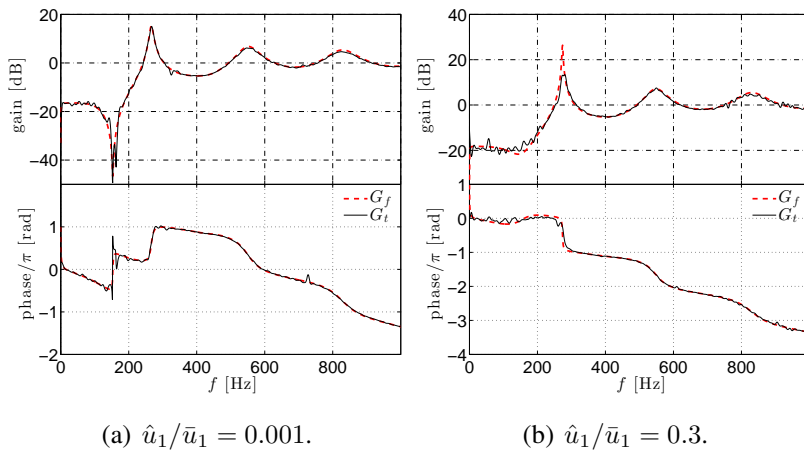
(a) $\hat{u}_1/\bar{u}_1 = 0.001$.

(b) $\hat{u}_1/\bar{u}_1 = 0.3$.

Figure 4. Comparison between the Bode diagrams for the OLTF obtained from time simulation G_t and analytical model G_f.
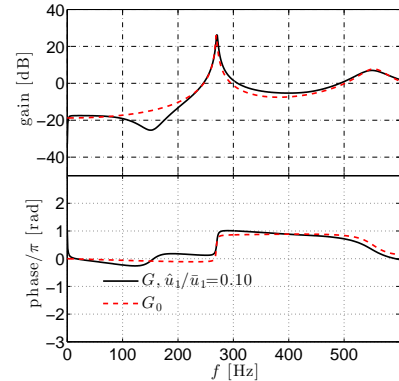
Figure 5. Comparison of the frequency response of G for $u_1'/\bar{u}_1 = 0.10$ and mathematical approximation.

[18]: (1) a control signal from a stabilizing feedback controller to eliminate the combustion instabilities; (2) a Gaussian white noise signal with equivalent amplitude to identify the OLTF for the required disturbance ratio $\hat{u}_1/\bar{u}_1$. Figure 4 shows the bode plots of OLTF for two $\hat{u}_1/\bar{u}_1$. The black solid line (G_t) indicates the results from our time domain simulation network model, while the red dashed line (G_f) represents the analytical OLTF obtained by combining the flame model and Eq. 6. The simulation results match perfectly with the analytical model, showing that our network model accurately reproduces the behavior of non-linear combustion instabilities.
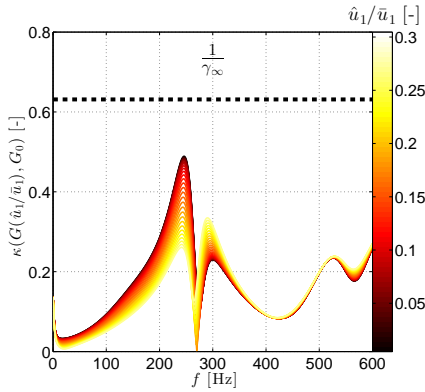
3.2 Controller design

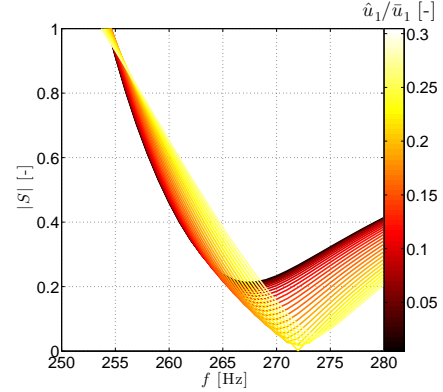**Figure 6.** Evolution of $\kappa(G(\hat{u}_1/\bar{u}_1), G_0)$ with frequency.

Figure 7. Evolution of S with frequency.

The $\mathcal{H}_\infty$ loop-shaping method is used in this work to design the controller [8], via the Matlab command $ncfsyn$. The resulting controller typically has the same order of the identified plant G. To obtain a low-order controller K, a fourth order approximate transfer function (Eq. 9) is used to fit the plant G for moderate velocity perturbations $\hat{u}_1/\bar{u}_1 = 0.1$.

$$G_0(s) = \frac{0.1562(s^2 - 3088s + 4.24 \times 10^6)(s^2 + 2734s + 6.01 \times 10^6)}{(s^2 - 15.2s + 2.86 \times 10^6)(s^2 + 298.8s + 1.21 \times 10^7)} \tag{9}$$

The comparison between the original plant G and the fitting transfer function G_0 is shown in Fig. 5. The fitted plot reproduces the unstable mode and the phase jump across this mode. The error between G_0 and G for different velocity disturbances $\hat{u}_1/\bar{u}_1$ can be measured by ν-gap [7] for single-input single-output system defined as:

$$\delta_\nu = \sup_{2\pi f} \kappa(G_0, G) = \sup_{2\pi f} \frac{|G_0(2\pi fi) - G(2\pi fi)|}{\left(1 + |G_0(2\pi fi)|^2\right)^{\frac{1}{2}} \left(1 + |G(2\pi fi)|^2\right)^{\frac{1}{2}}} \tag{10}$$

Figure 6 shows the plots of $\kappa(G_0, G)$ for different $\hat{u}_1/\bar{u}_1$ in the range $0 \leq \hat{u}_1/\bar{u}_1 \leq 0.3$. The dominant differences are located around the unstable frequency (270 Hz). The ν-gap denotes the upper bound of the difference between two $\mathcal{H}_\infty$ norms and the set of ν-gaps capture the range over which the functions $G(\hat{u}_1/\bar{u}_1)$ deviate from G_0. The ν-gap metric fits very naturally into the $\mathcal{H}_\infty$ loop-shaping synthesis framework, which returns both a feedback controller K (Eq. 11) and the corresponding "stability margin", $1/\gamma_\infty$, corresponding to this controller. When $\delta_\nu < 1/\gamma_\infty$, the controller is guaranteed to stabilize the entire set of plants G (for example the results shown in Fig. 6).

$$K(s) = \frac{-1.713(s - 7.51 \times 10^3)(s^2 - 846.1s + 1.03 \times 10^7)}{(s + 1.70 \times 10^4)(s^2 + 2362s + 8.08 \times 10^6)} \tag{11}$$

The sensitivity function is another measure of the performance of the controller and for positive feedback control is expressed as:

$$S(s) = G(s)\big|_{\text{control}} \Big/ G(s)\big|_{\text{no control}} = \frac{1}{1 - G(s)K(s)} \tag{12}$$
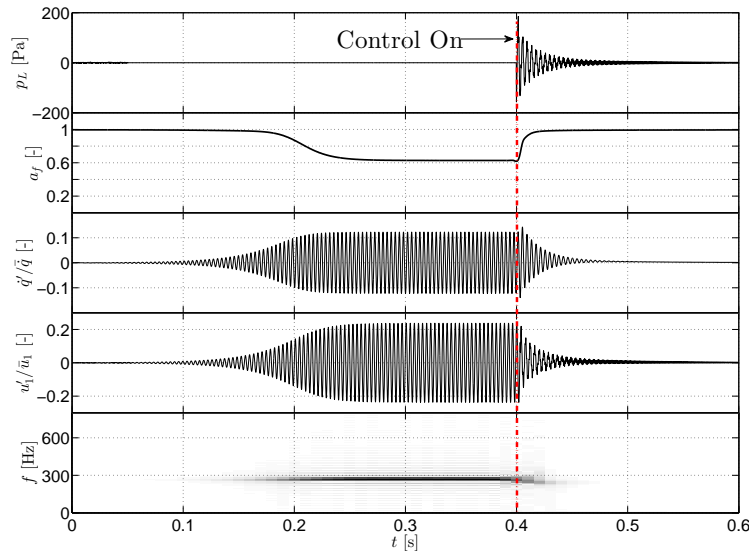
Figure 8. Evolution of the signals with time. From top to bottom: (1).Signal from the loudspeaker p_L; (2). gain a_f of the flame model; (3).heat release rate perturbations ratio $\dot{q}'/\bar{\dot{q}}$; (4).velocity perturbations ratio $u_1'/\bar{u}_1$. (5).Time-frequency analysis of $u_1'/\bar{u}_1$. The resolution: [0.01 s, 10 Hz].

When $|S(2\pi f^* i)| < 1$ (f^* denotes the unstable frequency), the feedback system is attenuating disturbances of the unstable mode compared to the open loop system. Figure 7 shows the plots of S for different $\hat{u}_1/\bar{u}_1$. The unstable frequency is from 265 to 275 Hz in the amplitude range $0 \leq \hat{u}_1/\bar{u}_1 \leq 0.3$. The fact that $|S(2\pi f^* i)| < 1$ at the oscillating frequency, means that the current controller will reduce the oscillation amplitude from within the limit cycle (at which point the plant appears as a "stable" plant due to saturation, see Fig. 4(b)). For sufficient attenuation, the plant will appear unstable (see Fig. 4(a)) and the controller will the stabilize the system.

The controller is implemented in time domain simulations. Fig. 8 shows the evolution of the signals with time when the controller is switched on. The perturbations of velocity and heat release rate decrease rapidly to weak white noise in 0.1 seconds once the controller is turned on. The loudspeaker signal is initially large in order to attain control and decreases to a much smaller value later to maintain control.

4. Conclusions

This article has presented a representative model for a non-linear combustion system exhibiting one unstable mode. The resulting time domain simulations have been seen to realistically reproduce the required non-linear behavior. A linear feedback controller which is theoretically guaranteed to stabilize the combustion system, even from within the non-linear limit cycle, has then been designed. This was achieved by combining the ν-gap metric, quantifying the difference between open loop plants, with $\mathcal{H}_\infty$ loop shaping robust controller design. As long as the ν-gap is smaller than the controller stability margin, the robust controller is guaranteed to stabilize the combustor for all possible non-linear flame responses. The resulting controller was applied to the unsteady combustion system while within a limit cycle, and was indeed found to suppress the combustion instability.

REFERENCES

[1] Candel, S. Combustion dynamics and control: Progress and challenges, *Proc. Combust. Inst.*, **29**(1), 1–28, (2002).

[2] Lieuwen, T.C. and Yang, V. Ed., *Combustion instabilities in gas turbines, Operational experience,*

Fundamental mechanisms, and Modeling, volume 210 of *Progress in Astronautics and Aeronautics*, AIAA, Inc., 2005.

3   Rayleigh, J.S.W, *The Theory of Sound*, Dover, New York, 1946.

4   Dowling, A.P. and Morgans, A.S. Feedback control of combustion oscillations, *Annu. Rev. Fluid Mech.*, **37**, 151–182, (2005).

5   Poinsot, T., Veynante, D., Bourienne, F., Candel, S., Esposito, E., and Surget, J. Initiation and suppression of combustion instabilities by active control, *Proc. Combust. Inst.*, **22**(1), 1363–1370, (1989).

6   Noiray, N., Durox, D., Schuller, T. and Candel, S. A unified framework for nonlinear combustion instability analysis based on the flame describing function. *J. Fluid Mech.*, **615**, 139–167, (2008).

7   Vinnicombe, G. *Uncertainty and Feedback: $\mathcal{H}_\infty$ loop-shaping and the ν-gap metric*. Imperial College Press, London, (2001).

8   McFarlane, D.C. and Glover, K. A loop shaping design procedure using $\mathcal{H}_\infty$ synthesis. *IEEE Transactions on Automatic Control*, **37**(6),759–769, (1992).

9   Dowling, A.P. The calculation of thermoacoustic oscillations. *J. Sound Vib.*, **180**(4), 557–581, (1995).

10   Marble, F.E. and Candel, S.M. Acoustic disturbance from gas non-uniformities convected through a nozzle. *J. Sound Vib.*, **55**(2), 225–243, (1977).

11   Morgans, A.S. and Annaswamy, A.M. Adaptive control of combustion instabilities for combustion systems with right-half plane zeros. *Combust. Sci. Tech.*, **180**(9), 1549–1571, (2008).

12   Levine, H. and Schwinger, J. On the Radiation of Sound from an Unflanged Circular Pipe. *Phys. Rev.*, **73**(4), 383–406, (1948).

13   Schuller, T., Durox, D. and Candel, S. A unified model for the prediction of laminar flame transfer functions: comparisons between conical and v-flame dynamics. *Combust. Flame*, **134**(1-2), 21–34, (2003).

14   Crocco, L. Aspects of Combustion Stability in Liquid Propellant Rocket Motors Part I: Fundamentals. Low Frequency Instability With Monopropellants. *Journal of the American Rocket Society*, **21**(6), 163–178, (1951).

15   Dowling, A.P. Nonlinear self-excited oscillations of a ducted flame. *J. Fluid Mech.*, **346**, 271–290, (1997).

16   Bellows, B.D, Zhang, Q., Neumeier, Y., Lieuwen, T., and Zinn, B.T. Forced response studies of a premixed flame to flow disturbances in a gas turbine combustor. *AIAA paper 2003-0824*, 2003.

17   Li, J. and Morgans, A.S. Thermoacoustic instabilities in the rijke tube: parametric study of linear stability and new insights into non-linear behaviour. *J. Sound Vib. (Submitted)*, 2014.

18   Morgans, A.S. and Dowling, A.P. Model-based control of combustion instabilities. *J. Sound Vib.*, **299**(1–2), 261–282, 2007.